IOP Publishing Journal of Physics B: Atomic, Molecular and Optical Physics
J. Phys. B: At. Mol. Opt. Phys. **53** (2020) 065303 (14pp) https://doi.org/10.1088/1361-6455/ab6621

Investigation into 3D-quantized ring vortices in rotating coupled atomic–molecular BEC

Sreoshi Dutta[1], **Krishna Rai Dastidar**[2,4] **and Chanchal Chaudhuri**[3]

[1] Dept. of Physics, Vivekananda College, Thakurpukur, Kolkata-700063, India
[2] School of Physical Sciences, Indian Association for the Cultivation of Science, Kolkata-700032, India
[3] Dept. of Physics, University of Gour Banga, Malda-732103, West Bengal, India

E-mail: spkrd@iacs.res.in

Received 9 October 2019, revised 4 December 2019
Accepted for publication 30 December 2019
Published 3 March 2020

Abstract

We study the coupled atomic–molecular quantized ring vortices of ^{87}Rb Bose–Einstein condensates trapped in a rotating 3D anisotropic cylindrical trap using both time-independent and time-dependent Gross–Pitaevskii approaches. For atomic to molecular conversion and vice versa, a two-photon Raman photoassociation scheme has been used. Atomic and molecular stationary state solutions show that the different number of nodes and crests formed in the density profile (as a function of r and z) for different combinations of radial ($\boldsymbol{n}$) and axial ($\boldsymbol{n_z}$) quantum numbers at a fixed azimuthal quantum number $\boldsymbol{l} = 2$, give rise to different structures around the 3D ring vortex centered at $r = 0$. We have considered both spontaneous and induced decays and compared the results with those without considering the decays. The out-of-phase oscillation of atomic and molecular numbers in two vortex states, both in the presence and absence of external decays, is the signature of coherence due to the atomic–molecular coupling. This coherence is also implemented in the evolution of coupled atomic and molecular vortices. The intensity of molecular ring vortices grows with time at the expense of that of atomic ring vortices, and vice versa. It is found that the intensity of the coupled atomic and molecular ring vortices starts to oscillate out of phase during evolution. Dependence of the atomic–molecular conversion efficiency and the lifetime of the system on the laser intensity of photoassociation lasers and the total number of atoms in two different vortex states reveals that the formation of atomic–molecular coupled vortices and the efficiency of formation can be controlled by varying these parameters. Linear stability analysis of vortex states as a function of different system parameters shows that the atomic vortices are more stable than molecular vortices, and the stable atomic and molecular vortices can be achieved by controlling these parameters.

Keywords: Bose–Einstein condensate, atomic–molecular coupled system, atomic–molecular coupled vortices, dynamics of coupled vortices in atomic–molecular BECS

1. Introduction

Experimental observations of atomic Bose–Einstein condensate (BEC) in trapped dilute gases [1] using laser light has led to many experimental and theoretical investigations into atomic BEC systems [1–5]. Experimental observations of the atomic vortex and its characterizations have been performed by different groups [6]. A number of theoretical works have been done to investigate atomic vortex [7], such as spontaneous shape deformation leading to the formation of a vortex, dynamics of vortex formation in merging BEC fragments, 'hidden' vortices in a rotating double well potential, the nucleation of spontaneous vortices in trapped Fermi gases undergoing a BCS–BEC crossover, 3D atomic vortex solitons, dynamics of single and multiple ring vortices, vortex-antivortex pairing in decaying superfluids, vortex formation in dipolar BEC, and recently active investigations on turbulence in trapped BEC. Dalfovo's group [7] have shown that after releasing the trap the core of quantized atomic vortices expands faster than the atomic cloud of BEC, which will facilitate the observation of atomic vortices by solving the Gross–Pitaevski equation numerically and comparing it with analytical results.

[4] Author to whom any correspondence should be addressed.

 © 2020 IOP Publishing Ltd Printed in the UK

Consequently, investigations into two-component BECs were started. Mathews *et al* observed vortices in two-component BECs and explored differences in the dynamics and stability of vortices [8]. Extensive theoretical studies [9] have been carried out to explore different aspects of two-component BECs e.g. considering dipole–dipole interaction, both attractive and repulsive atom–atom interactions, spin–orbit (SO)-coupling etc, using the Gross–Pitaevskii equation (GPE).

With the advent of studies on photoassociation (PA) processes in cold atoms and atomic BECs [10, 11], investigations into atomic–molecular coupled BEC systems have started. The formation of molecules from atomic BEC or ultracold atoms by PA was first introduced by Julienne's group [10] through a two-step process involving stimulated free–bound transition followed by spontaneous bound–bound emission, where the latter results in the production of an incoherent mixture of a large range of vibrational levels in the electronic ground state of the molecules. Hence stimulated bound–bound transition was chosen to achieve the state-specific population of the final molecular state of interest either through an adiabatic or a nonadiabatic pathway, which is essentially a stimulated two-photon Raman PA. Experimentally state selective molecules at rest have been created from atomic BEC by the PA process adopting the Raman two-photon stimulated free–bound and bound–bound transition technique [12, 13] and by the magnetoassociation process applying the Feshbach resonance technique [14–16]. This technique has also been used for condensation of molecular Fermi gases [17]. Many theoretical [18–24] attempts were also made to understand and set the guidelines for the realisation of molecular BECs using two-photon Raman PA, as well as magnetic Feshbach resonances. A number of theoretical efforts have been made to find out the enhancement of conversion efficiency through different approaches such as time-dependent magnetic field in conjunction with stimulated Raman transition [23], proper tuning of the pulse duration [24, 25] and the coherent population trapping in Feshbach resonance-assisted stimulated Raman adiabatic pathways [26, 27]. Dastidar's group [21] explored the coherences in the evolution of atomic and molecular density due to the atomic–molecular coupling via Raman two-photon association and by magnetic Feshbach resonance using a modified Gross–Pitaevskii approach in the coupled atomic–molecular BEC system, and the nature of out-of-phase oscillation of atomic and molecular density has been compared with experimental results.

The structure of vortices in two-species or two-component atomic condensates and its dependence on the system parameters have been studied [8, 9]. However, the studies of the formation of vortices in atomic–molecular coupled BEC systems are different from that of two-component atomic BEC systems due to the presence of atomic–molecular conversion coupling and the mass of molecules is twice that of atoms in the former. Some theoretical investigations have been carried out on the formation, structure and stability of vortices and vortex lattices in atomic–molecular coupled BEC systems. Julienne's group analyzed the structure and stability of vortices in hybrid atomic–molecular BEC using the Gross–Pitaevskii model, adopting the stimulated Raman-induced PA process [28]. They predicted new types of topological vortex states in coherently coupled two-component condensates even without a trap, and demonstrated the nontrivial dynamics of the coupled system in the presence of losses. Bigelow's group has studied the effect of atomic–molecular coupling on the formation and structure of vortex lattices in rotating atomic–molecular coupled BEC systems [29]. The structural phase transitions in this coupled system have been explored by studying the dependence of the degree of phase matching on the system parameters e.g. atomic–molecular coupling strength, atomic–molecular interaction and rotation frequency of the coupled system. Liu's group has explored the dependence of the nature of vortices on different combinations of quantum numbers, principal and secondary quantum numbers in a rotating atomic–molecular coupled BEC system, by using analytical solutions for vortices [30]. They have studied the formation of vortex lattices in atomic–molecular coupled BEC systems considering space modulated nonlinearity and the dependence of the structure of vortex lattices on the Raman detuning and atomic–molecular coupling strength. They have shown that atomic–molecular interaction plays a crucial role in controlling the structure of vortex lattices. However, to our knowledge, an experimental study has not yet been carried out on coupled atomic–molecular vortices.

In the present study we have investigated the dynamics, stability and control over the formation of atomic and molecular coupled vortices in a rotating coupled atomic–molecular BEC of ^{87}Rb atoms. In this scheme coherent $^{87}Rb_2$ molecules are obtained in the lowest vibrational level of the electronic ground state via two-photon Raman PA of ^{87}Rb atoms. Here the GPE with an additional rotational term has been used. For the formation of coupled atomic–molecular quantized vortices in the steady state, time-independent 3D coupled GP equations have been solved using the imaginary time method. The dependence of the structure and shape of the atomic and molecular vortices on the different combinations of radial and axial quantum numbers (due to the presence of nodes and crests in the density profiles) have been studied. To study the dynamics of these coupled vortices in 3D we have solved time-dependent coupled GP equations using the Crank–Nicholson method. It has been shown previously that atomic and molecular density in a (nonrotating) coupled atomic–molecular BEC system in the ground state oscillate coherently due to the presence of atomic–molecular conversion coupling [19, 21]. In this work we have explored the signature of coherences in the dynamics of atomic and molecular quantized 3D ring vortices (which are the excited states of the coupled system) in a rotating atomic–molecular coupled BEC system. The feasibility of formation and the stability of coupled atomic–molecular quantized vortices have been investigated by choosing different system parameters which are experimentally realizable.

In practice, external decays (spontaneous and induced) may play a crucial role in the stability of the coupled system. Hence spontaneous decay of excited atoms and the decay of molecules in two different channels (bound and the continuum of the ground state) induced by PA lasers have been considered. The dependence of conversion efficiency and the decay time of the total number of particles to $1/e$ times its

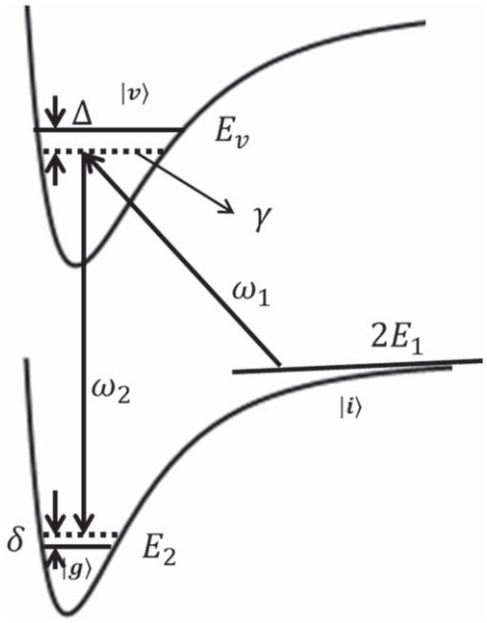

Figure 1. Schematic representation of two-photon Raman PA.

initial value on the initial number of atoms and the laser intensities have been studied considering the external decays. To investigate the stability of atomic and molecular vortices formed in different vortex states the imaginary part of the energy of the vortex states of atoms and molecules have been studied as a function of system parameters e.g. initial number of atoms, laser intensity, atomic–molecular interaction and the rotation frequency of the coupled system.

In this paper, the theoretical framework has been described in section 2. The theoretical formulation is given in section 2.1 and the numerical methods have been described in section 2.2. The results and discussions have been given in section 3. Results on the formation of vortices in the steady state have been given in section 3.1 and the results on the dynamics of atomic–molecular quantized vortices have been described in section 3.2. The variation in decay time of the system, atom to molecule conversion efficiency and the dependence of the stability of vortex states on different system parameters have been discussed in section 3.3. Finally the conclusions have been drawn in section 4.

2. Theoretical framework

2.1. Theoretical model

Figure 1 schematically shows the two-photon Raman PA scheme where two atoms initially in the state $|i\rangle$, of total energy $2E_1$, collide to form a molecule in the rovibrational state $|v\rangle$, of energy E_v, of an excited electronic state in the presence of the coupling laser field of frequency ω_1, which subsequently undergoes a transition to the ground state $|g\rangle$, of energy E_2, through stimulated emission by the second coupling laser of frequency ω_2. The two-photon Raman detuning is given as $\delta = (2E_1 - E_2)/\hbar - (\omega_2 - \omega_1)$ and the two-photon transition will be resonant when δ equals to zero.

In order to study the evolution of atomic and molecular vortices in rotating coupled atomic and molecular BECs, we solved the coupled GPE of motion for atoms (wavefunction ψ_a) and molecules (wavefunction ψ_m) as follows.

$$i\hbar\frac{\partial\psi_a}{\partial t} = \left[-\frac{\hbar^2\nabla^2}{2m} + U_a(r,z) + \lambda_a|\psi_a|^2 + \lambda_{am}|\psi_m|^2\right] \times \psi_a + \chi\psi_a\psi_m^* - i\hbar\alpha\psi_a - \hbar\beta_1\psi_a - i\hbar\Gamma_1|\psi_a|^2\psi_a + i\hbar\Omega\frac{\partial\psi_a}{\partial\theta} \quad (1)$$

$$i\hbar\frac{\partial\psi_m}{\partial t} = \left[-\frac{\hbar^2\nabla^2}{4m} + U_m(r,z) + \lambda_m|\psi_m|^2 + \lambda_{am}|\psi_a|^2 - \hbar\delta\right]\psi_m + \frac{\chi}{2}\psi_a\psi_a^* - \hbar\beta_2\psi_m - i\hbar\Gamma_2\psi_m + i\hbar\Omega\frac{\partial\psi_m}{\partial\theta} \quad (2)$$

where $U_a(r,z) = \frac{1}{2}m\omega_r^2(r^2 + \lambda^2z^2)$ and $U_m(r,z) = m\omega_r^2(r^2 + \lambda^2z^2)$ are the external anisotropic cylindrical harmonic trap potentials for atoms and molecules respectively, λ is the anisotropic factor $(=\frac{\omega_z}{\omega_r})$, where ω_r and ω_z are the angular trapping frequencies along radial and axial direction of the system, respectively. λ_a, λ_m, λ_{am} are the atom–atom, molecule–molecule and atom–molecule interaction strength, respectively. According to Bogoliubov mean field theory $\lambda_a = \frac{4\pi\hbar^2a}{m}$, where a is the s-wave scattering length for atom–atom interaction and we consider that $\lambda_a = \lambda_m = \lambda_{am}$ for simplicity. The spontaneous decay rate is denoted by α and Γ_1, Γ_2 indicate induced decay rates, β_1, β_2 represent the atomic and molecular light shift terms. Furthermore, $\tilde{\delta}$ is related to effective two-photon Raman detuning ($\tilde{\delta} = \delta + \beta_2 - 2\beta_1$) and Ω is the angular frequency of rotation of the system.The last terms in equations (1) and (2) represent the rotational energy terms producing vortices. χ is the atomic–molecular Raman coupling constant, i.e., the conversion factor from atom to molecule and vice versa.

The form of atomic–molecular Raman coupling is expressed as

$$\frac{\chi}{\hbar} = -\frac{\Omega_1\Omega_2}{2\sqrt{2}}\sum_v\frac{I_{1,v}I_{2,v}^*}{\Delta_v} \quad (3)$$

where Ω_1 is the free-bound and Ω_2 is the bound-bound Rabi frequencies, which are functions of laser intensities I_1 and I_2 respectively: $\Omega_{1,2} \propto \sqrt{I_{1,2}}$. The expression for the atom–atom scattering length can be written as

$$a = a_{bg} - \frac{m}{4\pi\hbar}\sum_v\left[\frac{{\Omega_1}^2}{4\Delta_v} + \frac{{\Omega_2}^2}{4\Delta_v^{(1)}}\right]|I_{1,v}|^2 \quad (4)$$

Here a_{bg} is the background scattering length, $I_{1,v}$ is the free-bound and $I_{2,v}{}'s$ are the bound-bound Frank–Condon factors. The spontaneous decay rate from an excited state of

an atom is

$$\alpha = \frac{\gamma_a}{8}\sum_{i=1,2}\frac{(D_i^A)^2}{D_i^2} \tag{5}$$

Two induced decay rates, atomic loss rates due to one photon association and the spontaneous Raman scattering rates for molecules are denoted as (stimulated)

$$\Gamma_j = \frac{\gamma_M}{8}\sum_v\left[\frac{(\Omega_j)^2}{\Delta_v^2} + \frac{(\Omega_{3-j})^2}{(\Delta_v^{(j)})^2}\right]|I_{j,v}|^2,\ (j = 1, 2) \tag{6}$$

The atomic and molecular light-shift terms are represented as, respectively,

$$\beta_1 = \sum_{i=1,2}\frac{(D_i^A)^2}{4D_i} \tag{7}$$

$$\beta_2 = \sum_v\left[\frac{(\Omega_2)^2}{4\Delta_v} + \frac{(\Omega_1)^2}{4\Delta_v^{(2)}}\right]|I_{2,v}|^2 \tag{8}$$

Here γ_a and γ_M are the spontaneous decay rates of atoms and molecules, respectively, $D_i = \omega_0 - \omega_i$ are the detuning of lasers from the resonant frequency ω_0 of the atomic transition between the dissociation limit of the ground and excited state energy. The expression for the respective detuning factors are given below,

$$\Delta_v = (E_v - 2E_1)/\hbar - \omega_1 \tag{9}$$

$$\Delta_v^{(1)} = (E_v - 2E_1)/\hbar - \omega_2 \tag{10}$$

$$\Delta_v^{(2)} = \frac{E_v - 2E_1}{\hbar} - \omega_1 \tag{11}$$

The above coupled GP equations (1) and (2) reduce to dimensionless GP equations by rescaling the length by linear harmonic oscillator length $a_{HO} = \sqrt{\hbar/m\omega}$, energy by $\hbar\omega$ and time by $1/\omega$ in a cylindrical polar coordinates system, as follow:

$$\begin{aligned} i\frac{\partial\psi_a}{\partial t} = &\left[-\frac{1}{2}\left(\frac{\partial^2}{\partial r^2} + \frac{1}{r}\frac{\partial}{\partial r} - \frac{l^2}{r^2} + \frac{\partial^2}{\partial z^2}\right)\right. \\ &\left. + \frac{1}{2}(r^2 + \lambda^2 z^2) + g_a|\psi_a|^2 + g_{am}|\psi_m|^2\right]\psi_a \\ &+ \frac{\chi}{\hbar}\psi_a\psi_m^* - i\alpha\psi_a - \beta_1\psi_a - i\Gamma_1|\psi_a|^2\psi_a \\ &+ i\Omega\frac{\partial\psi_a}{\partial\theta} \end{aligned} \tag{12}$$

$$\begin{aligned} i\frac{\partial\psi_m}{\partial t} = &\left[-\frac{1}{4}\left(\frac{\partial^2}{\partial r^2} + \frac{1}{r}\frac{\partial}{\partial r} - \frac{l^2}{r^2} + \frac{\partial^2}{\partial z^2}\right) + (r^2 + \lambda^2 z^2)\right. \\ &\left. + g_m|\psi_m|^2 + g_{am}|\psi_a|^2 + \epsilon\right]\psi_m + \frac{\chi}{2\hbar}\psi_a\psi_a^* \\ &- \beta_2\psi_m - i\Gamma_2\psi_m + i\Omega\frac{\partial\psi_m}{\partial\theta} \end{aligned} \tag{13}$$

We assume the form of the wave function $\psi(r, z, \theta, t)$, both for atom and molecule, as

$$\psi_i(r, z, \theta, t) = f_i(r, z)e^{il\theta - i\mu_i t} \tag{14}$$

where i corresponds to atoms and molecules. $\mu_i's$ are the chemical potentials, 'l' is the azimuthal quantum number also known as *intrinsic vorticity* and $f_i(r, z)$'s are the time-independent wavefunctions. Using the wavefunction from equation (14) in equations (12) and (13), the time-independent forms of the GP equations take the following forms

$$\begin{aligned} &\left[-\frac{1}{2}\left(\frac{\partial^2}{\partial r^2} + \frac{1}{r}\frac{\partial}{\partial r} - \frac{l^2}{r^2} + \frac{\partial^2}{\partial z^2}\right) + \frac{1}{2}(r^2 + \lambda^2 z^2)\right. \\ &\left. + g_a|f_a|^2 + g_{am}|f_m|^2\right]f_a + \frac{\chi}{\hbar}f_a f_m^* - l\Omega f_a = \mu_a f_a \end{aligned} \tag{15}$$

$$\begin{aligned} &\left[-\frac{1}{4}\left(\frac{\partial^2}{\partial r^2} + \frac{1}{r}\frac{\partial}{\partial r} - \frac{l^2}{r^2} + \frac{\partial^2}{\partial z^2}\right) + (r^2 + \lambda^2 z^2)\right. \\ &\left. + g_m|f_m|^2 + g_{am}|f_a|^2\right]f_m + \frac{\chi}{2\hbar}f_a f_a^* - l\Omega f_m = \mu_m f_m \end{aligned} \tag{16}$$

The approximate stationary state solutions of the equations (15) and (16), neglecting the nonlinearity of the system, can be written as [31]

$$f_a(r, z) \sim r^l L_n^l(r^2)e^{-\frac{1}{2}(r^2+\lambda z^2)}H_{n_z}(\sqrt{\lambda}z) \tag{17}$$

$$f_m(r, z) \sim r^l L_n^l(2r^2)e^{-(r^2+\lambda z^2)}H_{n_z}(\sqrt{2\lambda}z) \tag{18}$$

where the functions f_a and f_m involve Gaussian–Laugurre–Hermite functions and the corresponding chemical potentials are (as $\lambda_a = \lambda_m$)

$$\mu_{a,m} = 2n + 1 + l - l\Omega + \left(n_z + \tfrac{1}{2}\right)\lambda \tag{19}$$

2.2. Numerical approach

We obtained the numerical stationary state solutions for the atomic and molecular vortices in a coupled BEC system by solving the time-independent atomic–molecular coupled GP equations (15) and (16) using an imaginary time evolution method taking f_a and f_m as the initial wavefunctions. We reduce the nonlinear Schrödinger equations (NLSE), which have been used for our coupled system in its dimensionless form, replacing radial distance $r = a_{HO}r'$, axial distance $z = a_{HO}z'$ and time $t = \tau/\omega$, where $a_{HO} = \sqrt{\hbar/m\omega}$ as follows:

$$\begin{aligned} &\left[-\frac{1}{2}\left(\frac{\partial^2}{\partial r'^2} + \frac{1}{r'}\frac{\partial}{\partial r'} - \frac{l^2}{r'^2} + \frac{\partial^2}{\partial z'^2}\right) + \frac{1}{2}(r'^2 + \lambda^2 z'^2)\right. \\ &\left. + g_a|f_a|^2 + g_{am}|f_m|^2\right]f_a + \chi' f_a f_m^* - l\Omega' f_a = \mu_a f_a \end{aligned} \tag{20}$$

$$\left[-\frac{1}{4}\left(\frac{\partial^2}{\partial r'^2}+\frac{1}{r'}\frac{\partial}{\partial r'}-\frac{l^2}{r'^2}+\frac{\partial^2}{\partial z'^2}\right)+(r'^2+\lambda^2 z'^2)+g_m|f_m|^2+g_{am}|f_a|^2+\epsilon'\right]f_m+\frac{\chi'}{2}f_a f_a^*-l\Omega' f_m=\mu_m f_m \tag{21}$$

where μ_a and μ_m are the eigenvalues of the atomic and molecular time-independent NLSEs. In order to obtain the numerical solutions of the stationary state equations (20) and (21), we implement the imaginary time method as follows:

$$f_j(r', z', \tau+\Delta\tau)=(1-i\Delta\tau H'_j)f_j(r', z', \tau) \tag{22}$$

where H'_j denotes the Hamiltonian corresponding to the atomic and molecular coupled equation in its dimensionless form. Numerical iteration is performed using the length step 0.01 along both the direction r and z within the range (0 to 5) and (−5 to 5) respectively. To get the converged solution for atomic and molecular vortices, the convergence of the solution has been checked to be 10^{-6} for the wavefunction. The time step we have used in this imaginary time iteration is 5×10^{-8} and at each time step of imaginary time, the total number of atoms and double the number of molecules have been normalized to the total number of particles N i.e. $\int\int(|f_a|^2+2|f_m|^2)2\pi r'dr'dz'=N$.

To study the dynamical behaviour of atomic and molecular vortices in a coupled atomic–molecular system we have solved the time-dependent coupled GP equations by applying the steepest descent method in the Crank–Nicholson scheme. We assume the wavefunction is of the form $\psi=\phi/\sqrt{r}$ for the sake of simplicity of our cylindrical system and to solve the equations (12) and (13) we impose the boundary conditions, which are $\phi_{a,m}(r, z, t)\to 0$ *as* $r, z\to 0$; and $|\phi_{a,m}(r, z, t)|\to e^{-(r^2+\lambda z^2)/2}$*as* $r, z\to\infty$. Using the Crank–Nicholson scheme we discretise coupled atomic and molecular time-dependent nonlinear Schrödinger equations (12) and (13) (in dimensionless form) in both the radial and axial directions and hence we obtain a pair of dimensionless equations for atomic BEC as follows:

$$\begin{aligned}i\frac{\phi^{n+\frac{1}{2}}_{a,j,k}-\phi^{n}_{a,j,k}}{\Delta\tau}&=-\frac{1}{4h^2}[(\phi^{n+\frac{1}{2}}_{a,j+1,k}-2\phi^{n+\frac{1}{2}}_{a,j,k}+\phi^{n+\frac{1}{2}}_{a,j-1,k})\\&+(\phi^{n}_{a,j+1,k}-2\phi^{n}_{a,j,k}+\phi^{n}_{a,j-1,k})]+\left[\frac{1}{2}r_j^2+\frac{1}{2r_j^2}\right.\\&\times\left(l^2-\frac{1}{4}\right)+g_a\frac{|\phi^n_{a,j,k}|^2}{r_j}+g_{am}\frac{|\phi^n_{m,j,k}|^2}{r_j}\\&\left.-i\frac{\alpha}{2\omega}-\frac{\beta_1}{2\omega}-i\frac{\Gamma_1}{2\omega}\frac{|\phi^n_{a,j,k}|^2}{r_j}-l\Omega\right]\left(\frac{\phi^{n+\frac{1}{2}}_{a,j,k}+\phi^{n}_{a,j,k}}{2}\right)\\&+\frac{\chi}{\omega}\frac{\phi^{n*}_{a,j,k}\phi^{n}_{m,j,k}}{\sqrt{r_j}}\end{aligned} \tag{23}$$

$$\begin{aligned}i\frac{\phi^{n+1}_{a,j,k}-\phi^{n+\frac{1}{2}}_{a,j,k}}{\Delta\tau}&=-\frac{1}{4h^2}[(\phi^{n+1}_{a,j,k+1}-2\phi^{n+1}_{a,j,k}+\phi^{n+1}_{a,j,k-1})\\&+(\phi^{n+\frac{1}{2}}_{a,j,k+1}-2\phi^{n+\frac{1}{2}}_{a,j,k}+\phi^{n+\frac{1}{2}}_{a,j,k-1})]\\&+\left[\frac{1}{2}\lambda^2 z_k^2+-i\frac{\alpha}{2\omega}-\frac{\beta_1}{2\omega}-l\Omega\right]\left(\frac{\phi^{n+1}_{a,j,k}+\phi^{n+\frac{1}{2}}_{a,j,k}}{2}\right)\end{aligned} \tag{24}$$

and a pair of dimensionless equations for molecular BEC as follows:

$$\begin{aligned}i\frac{\phi^{n+\frac{1}{2}}_{m,j,k}-\phi^{n}_{m,j,k}}{\Delta\tau}&=-\frac{1}{8h^2}[(\phi^{n+\frac{1}{2}}_{m,j+1,k}-2\phi^{n+\frac{1}{2}}_{m,j,k}+\phi^{n+\frac{1}{2}}_{m,j-1,k})\\&+(\phi^{n}_{m,j+1,k}-2\phi^{n}_{m,j,k}+\phi^{n}_{m,j-1,k})]+\left[r_j^2+\frac{1}{4r_j^2}\left(l^2-\frac{1}{4}\right)\right.\\&\left.+g_m\frac{|\phi^n_{m,j,k}|^2}{r_j}+g_{am}\frac{|\phi^n_{a,j,k}|^2}{r_j}+\frac{\delta}{\omega}-\frac{\beta_2}{2\omega}-i\frac{\Gamma_2}{2\omega}-l\Omega\right]\\&\times\left(\frac{\phi^{n+\frac{1}{2}}_{m,j,k}+\phi^{n}_{m,j,k}}{2}\right)+\frac{\chi}{2\omega}\frac{\phi^{n*}_{a,j,k}\phi^{n}_{a,j,k}}{\sqrt{r_j}}\end{aligned} \tag{25}$$

$$\begin{aligned}i\frac{\phi^{n+1}_{m,j,k}-\phi^{n+\frac{1}{2}}_{m,j,k}}{\Delta\tau}&=-\frac{1}{8h^2}[(\phi^{n+1}_{m,j,k+1}-2\phi^{n+1}_{m,j,k}+\phi^{n+1}_{m,j,k-1})\\&+(\phi^{n+\frac{1}{2}}_{m,j,k+1}-2\phi^{n+\frac{1}{2}}_{m,j,k}+\phi^{n+\frac{1}{2}}_{m,j,k-1})]+\left[\frac{1}{2}\lambda^2 z_k^2+-i\frac{\alpha}{2\omega}\right.\\&\left.-\frac{\beta_1}{2\omega}-l\Omega\right]\left(\frac{\phi^{n+1}_{m,j,k}+\phi^{n+\frac{1}{2}}_{m,j,k}}{2}\right)\end{aligned} \tag{26}$$

where the discretized wavefunctions are $\phi^n_{i,j,k}=\phi_i(r_j z_k \tau_n)$; $i=a, m$, for atoms and molecules, respectively. Here the dimensionless r′, z′ and τ' have been substituted by r, z and τ for simplicity.

For numerical calculation, the stationary state solution obtained numerically by solving the time independent equations has been used as a wavefunction in the time-dependent equation at $t=0$. The maximum length in the radial and axial directions have been taken in units of a_{HO} is 5. We use the step size (h) along the radial and axial directions, which are the same, 0.01, and the time step ($\Delta\tau$) is 0.1 μs. The dynamics of the coupled system has been studied for 0.3 ms.

2.3. Linear stability analysis

For the linear stability analysis we consider the perturbed solution of equations (12) and (13), as follows.

$$\Psi_a=[\Phi_a(r, z)+u_1e^{i\lambda t}+w_1e^{-i\lambda t}]e^{-i\mu_a t} \tag{27}$$

$$\Psi_m=[\Phi_m(r, z)+u_2e^{i\lambda t}+w_2e^{-i\lambda t}]e^{-i\mu_m t} \tag{28}$$

where $|u_1| \ll 1$, $|u_2| \ll 1$, $|w_1| \ll 1$ and $|w_2| \ll 1$ are the small perturbations, neglecting the higher order term. Substituting these wave functions (27) and (28) into the equations (12) and (13), we get the following eigenvalue equation with eigenvalue λ.

$$\begin{bmatrix} L_1 & \sqrt{2}\chi\Phi_m - g_a\Phi_a^2 + i\Gamma_1\Phi_a^2 & \sqrt{2}\chi\Phi_a - g_{am}\Phi_a\Phi_m & -g_{am}\Phi_a\Phi_m \\ g_a\Phi_a^2 - i\Gamma_1\Phi_a^2 - \sqrt{2}\chi\Phi_m & -L_1 & g_{am}\Phi_a\Phi_m & g_{am}\Phi_a\Phi_m - \sqrt{2}\chi\Phi_m \\ \sqrt{2}\chi\Phi_a - g_{am}\Phi_a\Phi_m & -g_{am}\Phi_a\Phi_m & L_2 & -g_m\Phi_m^2 \\ g_{am}\Phi_a\Phi_m & g_{am}\Phi_a\Phi_m - \sqrt{2}\chi\Phi_a & g_m\Phi_m^2 & -L_2 \end{bmatrix} \begin{bmatrix} u_1 \\ w_1 \\ u_2 \\ w_2 \end{bmatrix} = \lambda \begin{bmatrix} u_1 \\ w_1 \\ u_2 \\ w_2 \end{bmatrix} \tag{29}$$

The matrix elements L_1 and L_2 are defined as

$$L_1 = \frac{1}{2}\left(\frac{\partial^2}{\partial r^2} + \frac{\partial^2}{\partial z^2} - \frac{\partial}{r\partial r}\right) - 2g_a\Phi_a^2 - g_{am}\Phi_m^2 - \frac{1}{2}(r^2 + \lambda^2 z^2) + \mu_a + l\Omega + i\alpha + \beta_1 \tag{30}$$

$$L_2 = \frac{1}{4}\left(\frac{\partial^2}{\partial r^2} + \frac{\partial^2}{\partial z^2} - \frac{\partial}{r\partial r}\right) - 2g_m\Phi_m^2 - g_{am}\Phi_a^2 - \frac{1}{4}(r^2 + \lambda^2 z^2) + \mu_m + l\Omega - \delta + i\Gamma_2 + \beta_2 \tag{31}$$

We solved the eigenvalue equation (29) to get the eigenvalues. If the eigenvalues are purely real then the wavefunctions are stable, otherwise they are unstable.

3. Results and discussion

In the two-photon Raman PA scheme used here the formation of the $^{87}Rb_2$ molecules is considered to be in the lowest vibrational level of the ground state $^3\Sigma_u^+(V_g(R))$ via 0_g^- excited state ($V_e(R)$) by association of two ^{87}Rb atoms from the continuum of the ground state (figure 1). The parameters used in these calculations are $\gamma_A = 3.7 \times 10^7\,S^{-1}$, $\gamma_M = 2\gamma_A$, $\Omega_1 = 2.3 \times 10^{10}\,S^{-1}$ $\Omega_2 = 6.324\times 10^9\,S^{-1}$, $\chi/\hbar = 7.6 \times 10^{-7}\,m^{3/2}s^{-1}$, $\Gamma_1 = 1.629 \times 10^{-23}\,m^3s^{-1}$, $\Gamma_2 = 304.4\,s^{-1}$, $\beta_1 = 2.108 \times 10^7\,s^{-1}$, $\beta_2 = 3.344 \times 10^6\,s^{-1}$, $\alpha = 134.06\,s^{-1}$, $\delta = 3.879 \times 10^7\,s^{-1}$ [19] unless otherwise mentioned. In this calculation the effective detuning delta-tilde (which includes the Ac Stark shift, β_1, β_2 and the two-photon Raman detuning, delta) has been kept fixed. The s-wave scattering length is 5.4 nm [21]. We have started with the initial number of atoms $N = 50\,000$ unless another variation of N is considered. The frequency of cylindrically symmetric harmonic trap potential in the radial direction has been taken as $\omega_r/2\pi = 100$ Hz, whereas in the axial direction the frequency $\omega_z = 0.36\omega_r$ [21]. The angular frequency of rotation of the condensate system has been taken as $\Omega = 0.6\omega_r$. For the sake of simplicity we have considered the strengths of all three interactions, atom–atom, molecule–molecule and atom–molecule are equal, i.e., $\lambda_a = \lambda_m = \lambda_{am}$ unless otherwise the interactions are varied to study the dependence of results on the particle-particle interactions.

3.1. Formation of vortices

To demonstrate the formation of quantized vortices in the rotating coupled atomic–molecular condensate, we obtained the stationary state solutions of time-independent rotating coupled GP equations (15) and (16) numerically, using the imaginary time evolution method, taking the Gaussian–Laguerre–Hermite functions as initial wavefunctions (equations (17) and (18)). The iteration has been continued until the convergence of wavefunctions reaches 10^{-6}.

Results of stationary state solutions have been shown in figure 2 for different values of radial (n) and axial (n_z) quantum numbers for a fixed value of azimuthal quantum number (l). Figures 2(a) and (b) show the plot of density profiles ($|\Phi_{a,m}(r, z)|^2$) as a function of r and z (in the units of a_{HO}) for atoms and molecules, respectively, for different values of radial and axial quantum numbers (n and n_z) for a fixed azimuthal quantum number $l = 2$. It is found that with the increase in n, the number of nodes in the density profile along the r-axis increases for a fixed value of n_Z. However, with the increase in n_z the density profile (crest and trough structure) obtained for the particular value of n is replicated or repeated n_z times along the z-axis, giving rise to the total number of nodes along the r-axis, $k = (n + 1)(n_z + 1)$, including the node (minimum) at $r = 0$, for a fixed value of $l = 2$. It is to be noticed that due to this replication or repeatation along the z-axis, minima in the density profile are developed along the z-axis. The central vortex appears around $r = 0$ line.

Corresponding 3D ring vortices for atoms and molecules have been plotted in figures 2(c) and (d), respectively. It is evident from these two figures that different combinations of radial (n) and axial (n_z) quantum numbers for a fixed value of azimuthal quantum number $l = 2$ give rise to a different structure of ring vortices and are centred at the $r = 0$ line. With the increase in the number of nodes and crests in the atomic density profile with the increase in n for a fixed value of n_z (as shown in figure 2(a)), more layers of crests and troughs are added around the central vortex, giving rise to a different structure around the central vortices, as shown in

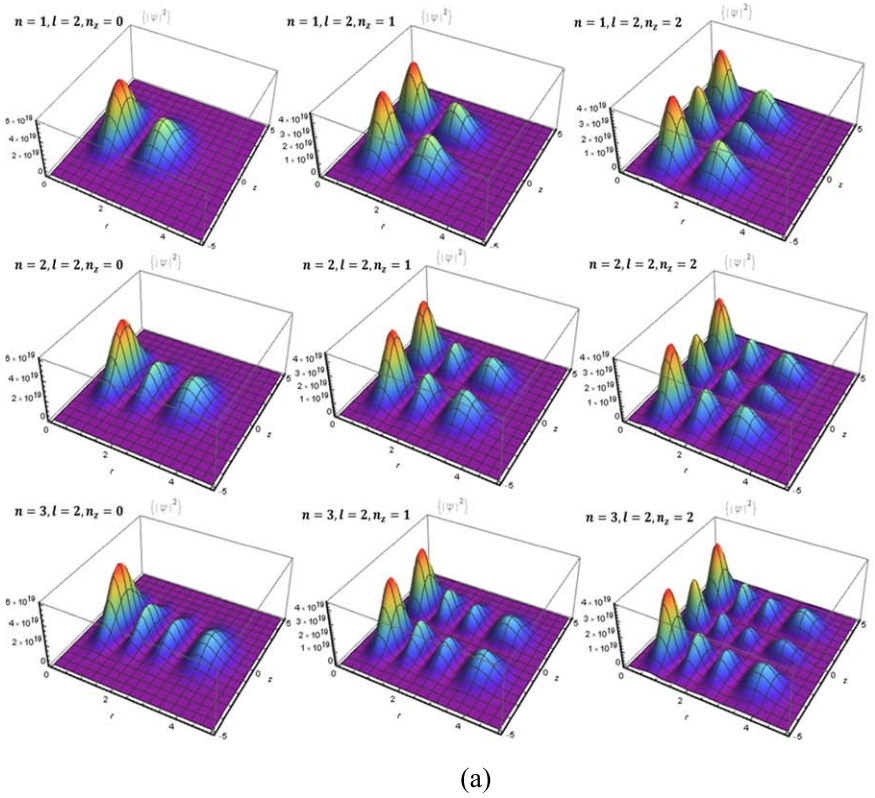

(a)

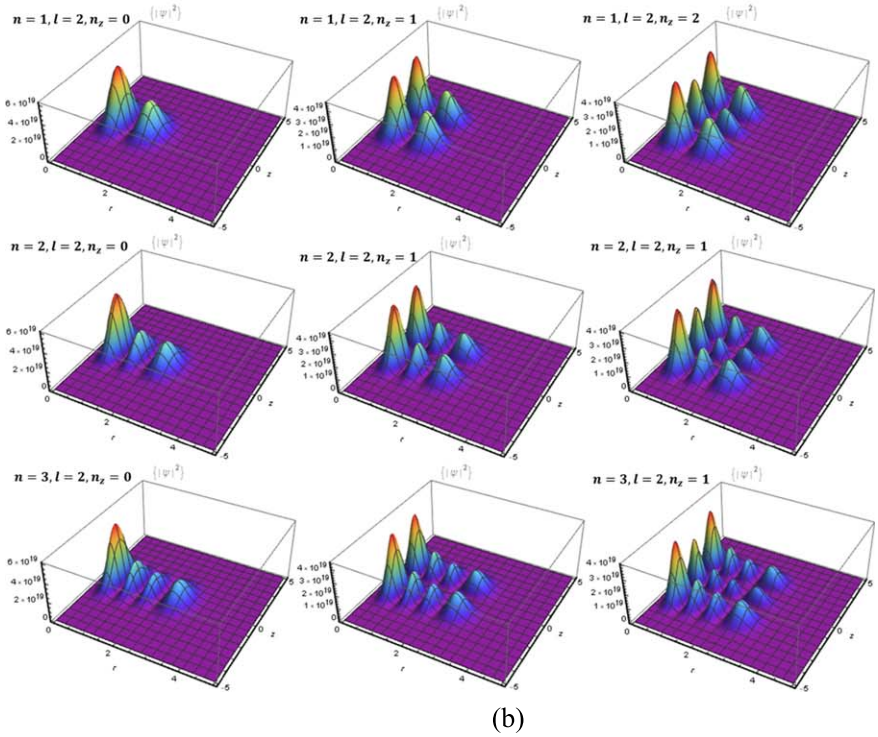

(b)

Figure 2. (a) Atomic density $|\Phi_a(r, z)|^2$ of the stationary state vortex solution for 3D coupled BEC system as a function of radial distance r (unit of a_{HO}) and axial distance z (unit of a_{HO}) for different combinations of radial (n) and axial (n_z) quantum numbers keeping azimuthal quantum numbers (l) fixed at 2. (b) Molecular density $|\Phi_m(r, z)|^2$ of the stationary state vortex solution for 3D coupled BEC system as a function of radial distance r (unit of a_{HO}) and axial distance z (unit of a_{HO}) for different combinations of radial (n) and axial (n_z) quantum numbers keeping azimuthal quantum numbers (l) fixed at 2. (c) Atomic vortices for different combinations of radial (n) and axial (n_z) quantum numbers for a fixed azimuthal quantum number $l = 2$. (d) Molecular vortices for different combinations of radial (n) and axial (n_z) quantum numbers for a fixed azimuthal quantum number $l = 2$.

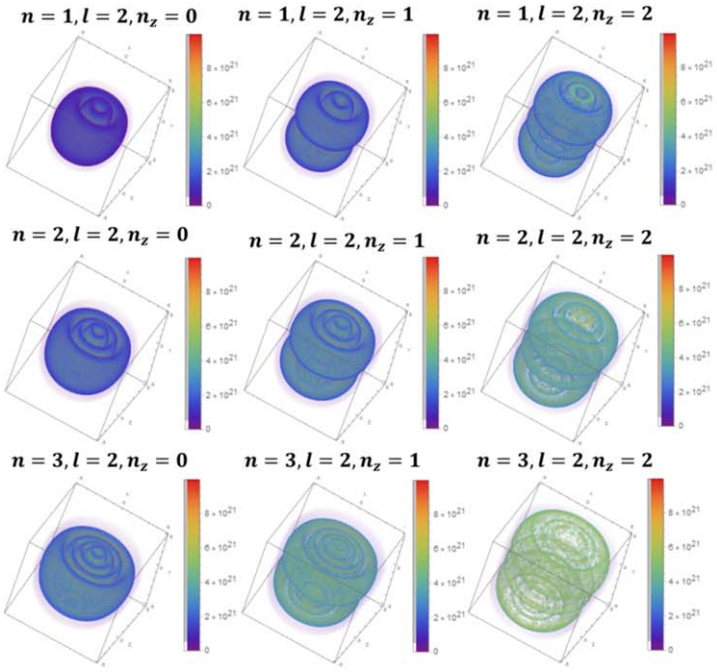

(c)

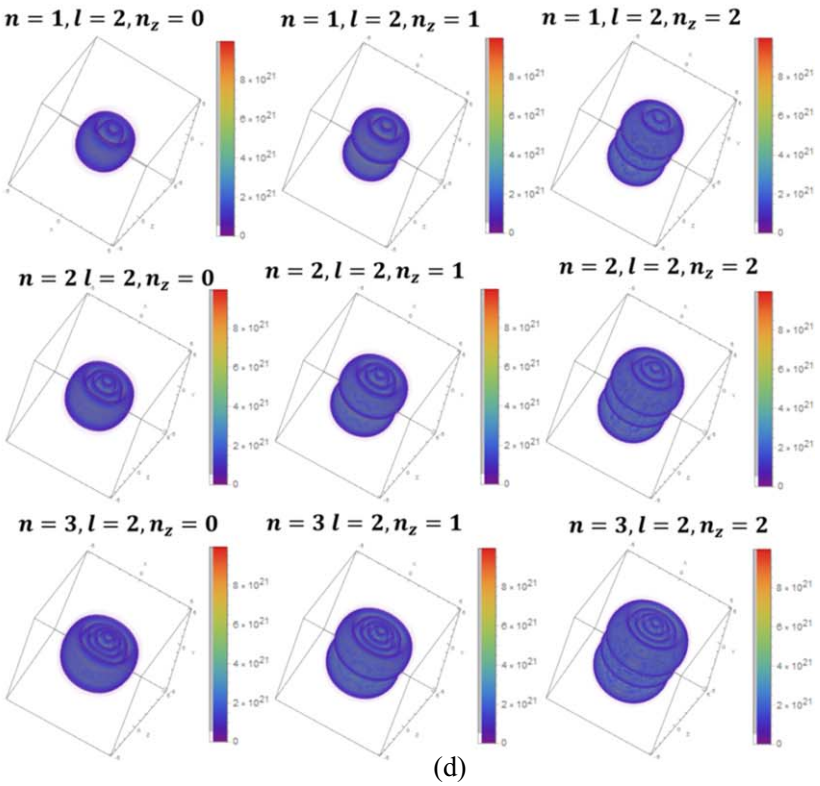

(d)

Figure 2. (Continued.)

figure 2(c). A similar feature has been obtained previously for atomic ring vortices for $n_z = 0$ by Li *et al* [7]. However, with an increase in n_z, the 3D ring vortex structure obtained for a fixed value of n is replicated or repeated $(n_z + 1)$-fold in the vertical direction (centred at the $r = 0$ line). Figure 2(d) shows that the same structure of molecular ring vortices as that of atomic vortices appear for different combinations of n and n_z and for $l = 2$. A comparison of these two figures shows that the molecular vortices are localized to a smaller region in comparison to atomic vortices by an amount $(1/\sqrt{2})$ due to a greater mass, which is twice that of the atom.

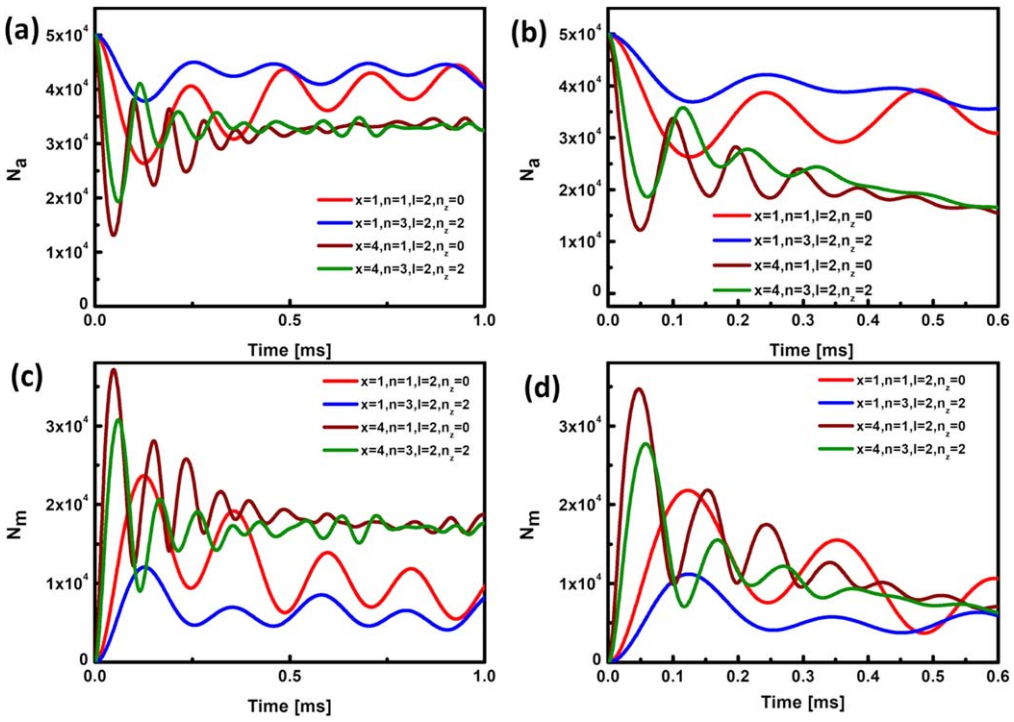

Figure 3. Variation of atomic (a) and molecular (c) number with time for $x = 1$ and $x = 4$ with decay $= 0$ for two different combinations of radial quantum number ($n = 1,3$) and axial quantum number ($n_z = 0,2$) with azimuthal quantum number fixed at $l = 2$ and the variation of atomic (b) and molecular (d) numbers with time for the same combination of n, l and n_z with external decay.

3.2. Evolution of vortices

We studied the formation and evolution of atomic and molecular vortices by solving the time-dependent coupled equations (12) and (13) using the steepest-descent method in the Crank–Nicholson scheme, with and without the external decay term.

Figure 3 illustrates the variations of the number of atoms and molecules in figures 3(a) and (c), respectively, with time for $x = 1$ and $x = 4$ without any decay at two different combinations of radial and axial quantum numbers (i) $n = 1$, $n_z = 0$ and (ii) $n = 3$, $n_z = 2$ at a fixed value of azimuthal quantum number $l = 2$. These two figures show there exists coherence in the oscillation of atomic and molecular numbers in two different vortex states leading to out-of-phase oscillations of atomic and molecular numbers with time due to the presence of atomic–molecular coupling in this coupled system. For a larger intensity of lasers i.e. $x = 4$, the oscillation frequency increases due to the increase in the Rabi frequency between states coupled by the lasers I_1 and I_2, but the coherence is maintained in the atomic and molecular number oscillations. Furthermore, the amplitude of oscillation is large for a lower vortex state ($n = 1$, $n_z = 0$) for a fixed x (compare blue and red lines with olive and wine lines) both in the case of atomic and molecular vortices.

It is found that with the inclusion of external decay (figures 3(b) and (d)), the nature of oscillations are the same and coherence is preserved, but the amplitude of oscillations die out much faster than that in the absence of decay. The damping in amplitude of oscillations is larger in the higher vortex state ($n = 3$, $n_z = 2$) than that in the lower vortex state ($n = 1$, $n_z = 0$), both in atomic and molecular cases for both the values of x. Moreover, for higher intensity ($x = 4$) the damping in oscillation is largely due to the increase in the induced decay, with the increase in intensity for both the species in two vortex states. Therefore we show that the coherence in number oscillation is present in the evolution of rotating atomic–molecular condensate system coupled by two-photon Raman PA in different vortex states, similar to that in the nonrotating coupled BEC in the ground state [21].

Figure 4 shows the evolution of coupled atomic and molecular quantized 3D ring vortices in the vortex state for $n = 3$, $l = 2$, $n_z = 2$ at different times without external decay (figure 4(a)) and with external decay (figure 4(b)) considering $x = 4$ for both the cases. In figures 4(a) and (b) we have also shown how the number of atoms and molecules oscillate out of phase with time in this vortex state without and with external decay, respectively. Comparing the set of figures for atomic vortices at different times with the corresponding molecular vortices at the same time, it is found that the intensity of crests of the molecular vortices grows at the expense of that for atomic vortices and vice versa. This feature is present for both the cases, without and with external decay. However, faster decay of the intensity of the crests is found in coupled ring vortices in the presence of external decay than that in the absence of it. Therefore, the signature of coherence is found to be implemented on the evolution of coupled atomic and molecular ring vortices.

3.3. Stability analysis

The variations of conversion efficiency (η) of atoms into molecules and the lifetime (τ) of the system (time for the

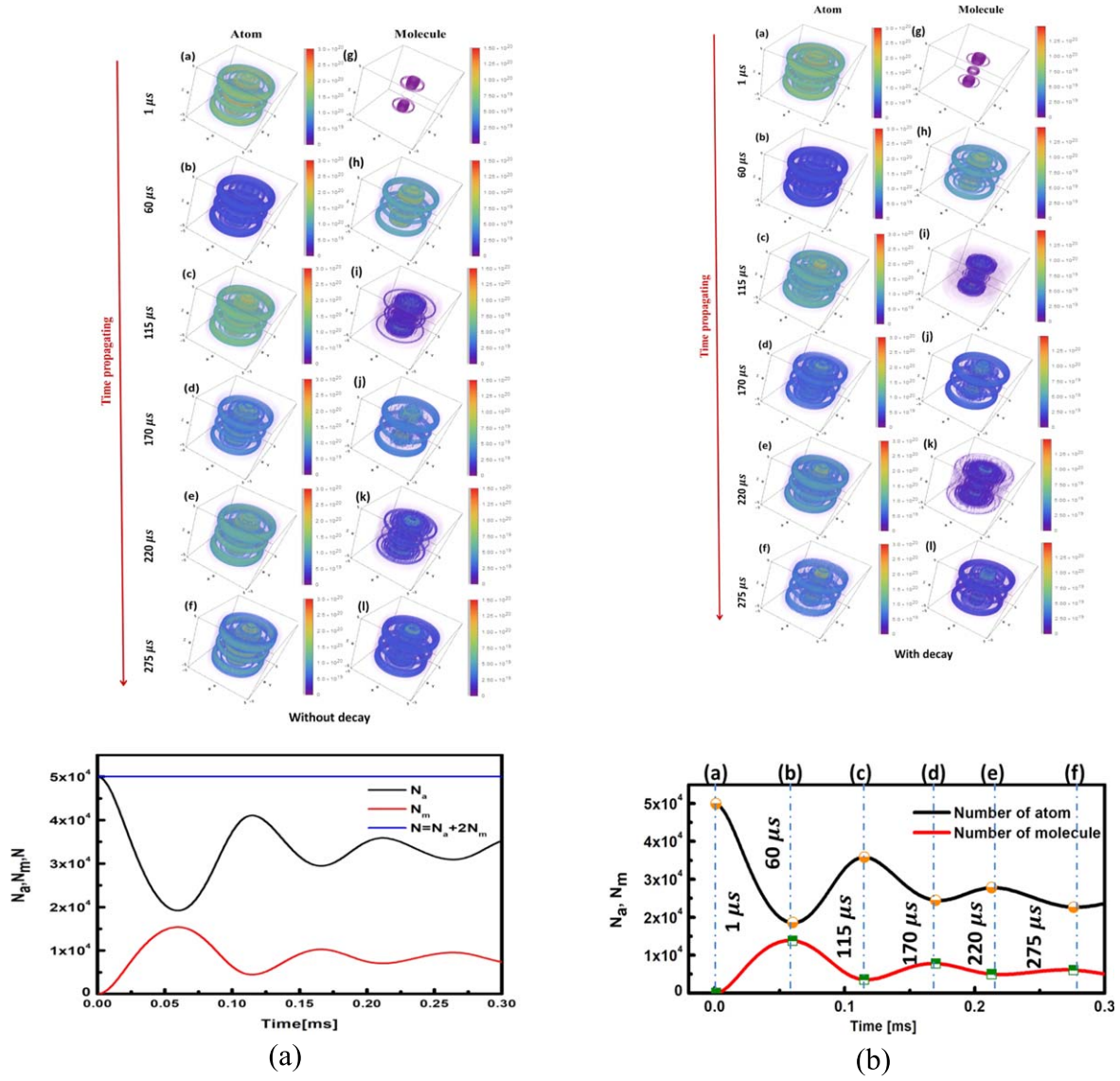

Figure 4. Evolution of coupled atomic and molecular 3D ring vortices in the vortex state for $n = 3$, $l = 2$, $n_z = 2$ at different times (a) without and (b) with external decay for atom (on the left) and for molecule (on the right) for $x = 4$ and $N = 50\,000$. Evolution of number of atoms and molecules with time for $n = 3$, $l = 2$, $n_z = 2$ vortex state has also been shown below that of the corresponding ring vortices.

decay of the total number of atoms to $1/e$ times its initial number) with x and the total number of atoms N in two vortex states in the presence of external decays (both spontaneous and induced decay) are presented in figure 5. The dependence of efficiency of conversion from atoms to molecules and the lifetime for two different vortex states as a function of x are shown in figures 5(a) and (c) respectively. For both the vortex states ($n = 1$, $l = 2$, $n_z = 0$ and $n = 3$, $l = 2$, $n_z = 2$) the variation of conversion efficiency and the lifetime with x show opposite nature, conversion efficiency sharply increases to saturation, whereas lifetime sharply decreases to a small value with the increase in x. Conversion efficiency is saturated in the lower vortex states after $x = 8$, while it starts to saturate from $x = 15$ for higher vortex states. It is also found that efficiency of conversion is lower for higher energy vortex states ($n = 3$, $l = 2$, $n_z = 2$), which is separated by an energy of about 2.6 in units of $\hbar\omega$ from the lower state. However, the decay rate is the same for both the vortex states. The variation in conversion efficiency and the lifetime with N are shown in figures 5(b) and (d), respectively. Similar to the variation with x (figures 5(a) and (c)), conversion efficiency increases and the lifetime decreases with increase in N. The rate of increase of conversion efficiency is higher for the lower vortex state than that for the higher vortex state (figure 5(b)), whereas the rate of decrease of lifetime is higher for the lower vortex state than that for the higher vortex state with an increase in N (figure 5(d)).

Conversion efficiency curves (solid lines in figures 5(a) and (b)) are obtained by fitting the calculated points shown in the figures. In figure 5(a) the fitted efficiency curve follows the relation with x as $\eta = A(1 - e^{-bx})$, where 'A' and 'b' are constants (table 1) and they depend on the initial number of atoms and the energy of the system. Furthermore, the variation of conversion efficiency with initial particle numbers follow a similar trend as it changes with x (i.e. $\eta = A(1 - e^{-bN})$)

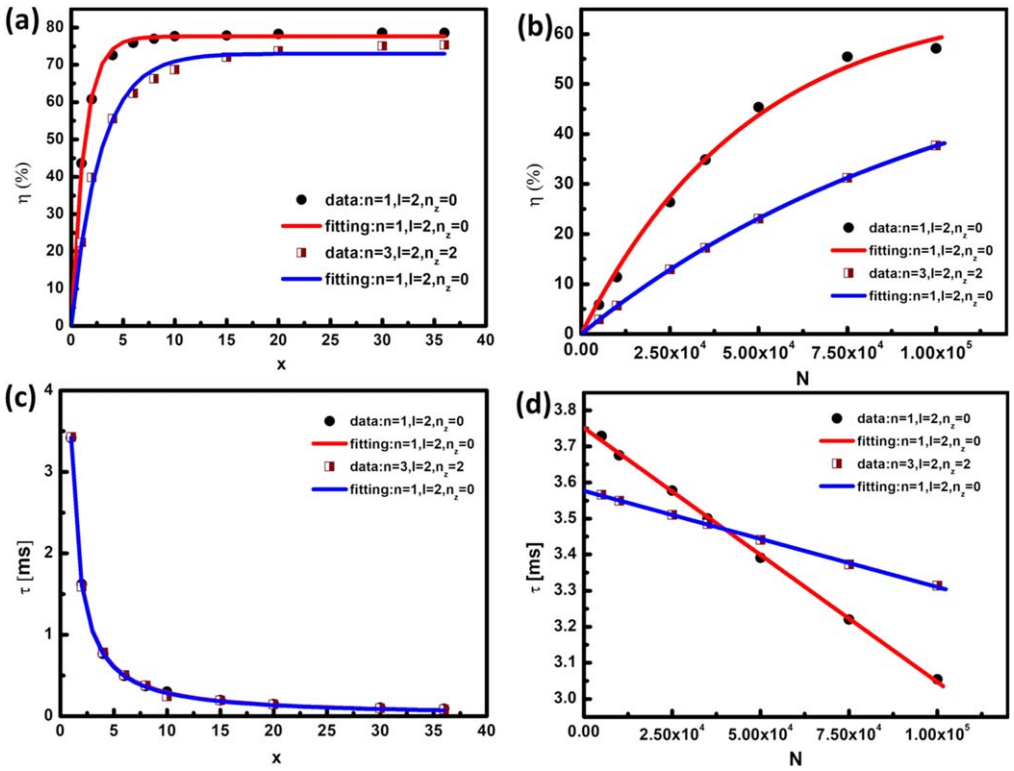

Figure 5. Variation of (a) conversion efficiency of atoms into molecules and (c) average lifetime with x (light intensity factor) for two different vortex states $n = 1$, $l = 2$, $n_z = 0$ (red line) and $n = 3$, $l = 2$, $n_z = 2$ (blue line). Variation of (b) conversion efficiency and (d) lifetime for vortex states with the quantum numbers $n = 1$, $l = 2$, $n_z = 0$ (red) and $n = 3$, $l = 2$, $n_z = 2$ (blue) for $x = 1$, with total number of particles (N). Here $\lambda_a = \lambda_m = \lambda_{am.}$. Results of calculations are given as points and the lines are from curve fittings.

Table 1. Fitting parameters for the conversion efficiency (η) and average lifetime (τ) of the system with x and N.

X variable	Y variable	Energy level	Parameter (1)	Parameter (2)
x	η	$n = 1, l = 2, n_z = 0$	$A = 77.62$	$b = 0.784$
x	η	$n = 3, l = 2, n_z = 2$	$A = 73.01$	$b = 0.355$
N	η	$n = 1, l = 2, n_z = 0$	$A = 67.33$	$b = 2.10 \times 10^{-5}$
N	η	$n = 3, l = 2, n_z = 2$	$A = 62.33$	$b = 9.26 \times 10^{-6}$
x	τ	$n = 1, l = 2, n_z = 0$	$A = 3.42$	$d = 1.069$
x	τ	$n = 3, l = 2, n_z = 2$	$A = 3.42$	$d = 1.082$
N	τ	$n = 1, l = 2, n_z = 0$	$A = 3.75$	$b = -7.04 \times 10^{-6}$
N	τ	$n = 3, l = 2, n_z = 2$	$A = 3.58$	$b = -2.67 \times 10^{-6}$

(figure 5(b)). The curve fitting of calculated data points shows the variation of the average lifetime of the particles with 'x' as $\tau = \mathrm{A/x^d}$ (figure 5(c)), where d is slightly greater than unity (table 1). But the lifetime of the system falls linearly with N ($\tau = A + bN$) (figure 5(d)) unlike its variation with x. The tabulated fitting parameters in table 1 shows that for η versus x and η versus N variations, the constant A is lower for higher vortex states while the constant b is double for the lower state than that of the higher state. For τ versus x variation of both the constants A and b are the same for both the lower and higher states. For τ versus N the variation of constant A is almost the same for both the lower and upper states, and the value of b is larger for the lower vortex state.

In the study of the formation and evolution of coupled atomic and molecular vortices in the rotating atomic–molecular BEC system, it is necessary to investigate the stability of such a system. It is known that the stability of the atomic and molecular vortices are inversely proportional to the value of the imaginary part of the energy of atomic and molecular vortex states $\mathrm{Im}(E_{a,m})$. To demonstrate the stability of atomic and molecular vortices in a rotating coupled system we have plotted $\mathrm{Im}(E_{a,m})$ for two different vortex states (figure 6). Figures 6((a)–(d)) provide the variation of $\mathrm{Im}(E_{a,m})$ for both the atomic and molecular vortex states with respect to x, N, λ_{am}/λ_a and Ω/ω_r, respectively. In the stability analysis, the effect of external decay has been considered. Variation of $\mathrm{Im(E_{a,m})}$ with x (figure 6(a)) shows that atomic vortices in both the energy states are almost stable. But the stability of molecular vortices decreases sharply in the lower energy state than that in the higher energy state. It is shown in figures 5(a) and (c) that the conversion efficiency and the lifetime behave oppositely with an increase in x and hence it will contribute to

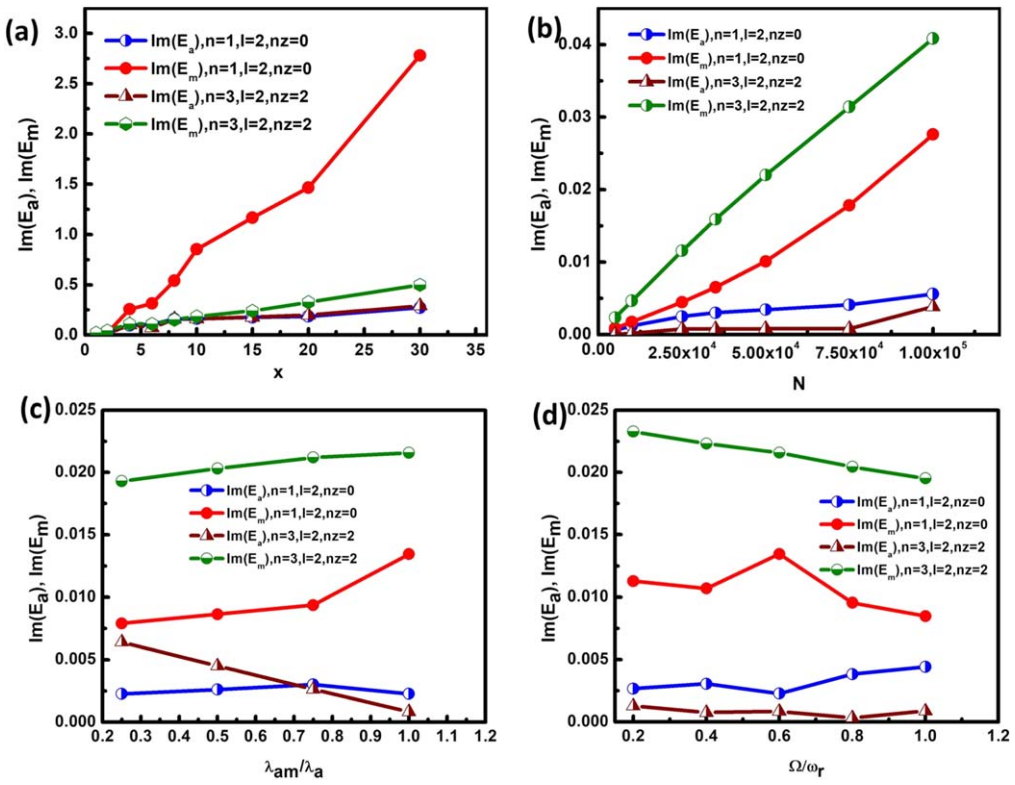

Figure 6. Stability curve for atom (blue and wine line) and molecule (red and olive line) with the variation of (a) x, (b) N, (c) relative interaction strengths $\lambda_{\rm am}/\lambda_{\rm a}$ and (d) external rotating frequency to trap frequency Ω/ω_r for vortex states with $n = 1$, $l = 2$, $n_{\rm z} = 0$ (blue and red lines) and $n = 3$, $l = 2$, $n_{\rm z} = 2$ (wine and olive line). Here $x = 1$ for N, $\lambda_{\rm am}/\lambda_{\rm a}$ and Ω/ω_r variation curves.

the energy of the system oppositely. With the increase in x the rate of increase of conversion efficiency, i.e. the rate of formation of molecules, is higher for the lower vortex state whereas the rate of decay of the system is the same for both the states. By repeating the calculation using a lower value of conversion efficiency (1/4 of its original value) we found that the stability of the lower state increases (not shown here). Thus a higher value of conversion efficiency of a lower state may give rise to the instability for the lower molecular vortex state higher than that for the upper molecular vortex state when the decay rate of both the states are the same.

Figure 6(b) shows that atomic vortices are stable with N whereas the stability of molecular vortices decreases with the increase in the total number of particles and the stability is much less than that of the atomic vortices. The dependence of stability on the strength of atomic–molecular interaction in the units of atom–atom interaction shows (figure 6(c)) that atomic vortices are stable for both the vortex states although that, in the higher energy state, increases slowly with an increase in atomic–molecular interaction. However, the stability of molecular vortices is much less than that of atomic vortices and it becomes more unstable with an increase in atomic–molecular interaction. The stability of molecular vortices in the lower state is greater than that of the higher state by a factor of two in the range $\lambda_{\rm am} \leqslant \lambda_{\rm a}$. Similarly, an increase in rotation frequency in units of trap frequency (figure 6(d)) shows stable atomic vortices and the stability is much more than that of the molecular vortices. The stability of molecular vortices in the lower state is double that in the higher state in the range $\Omega \leqslant \omega_r$. These figures reveal that although atomic vortices are stable in both the energy states, and more or less independent of system parameters (x, N, $\lambda_{\rm am}/\lambda_{\rm a}$ and Ω/ω_r), stability of molecular vortices is less than that of atomic vortices and it decreases with the increase in these system parameters, except for rotation frequency. With an increase in Ω/ω_r, molecular stability slightly increases. Moreover, the stability in the higher energy vortex state is lower than that in the lower energy vortex state, except in the variation with x. Therefore the stability of atomic and molecular ring vortices in a coupled rotating atomic–molecular BEC system can be controlled by varying different system parameters such as the intensity of PA lasers, the initial number of atoms, interaction strengths and the rotation frequency of the system.

4. Conclusion

A detailed investigation into the rotating coupled atomic–molecular BECs of ^{87}Rb trapped in a 3D-anisotropic cylindrical trap, in both time-independent and time-dependent Gross–Pitaevskii approaches, reveal that coupled atomic and molecular quantized ring vortices can be achieved in a coupled BEC system. For different combinations of radial (n) and axial (n_z) quantum numbers at a fixed azimuthal quantum number (l) different numbers of nodes are obtained in the density profile (as a function of r and z). The presence of these nodes and crests in the density profile give rise to different structures around the central

vortex at $r = 0$. Although the structure of vortices formed for a particular combination of n, n_z and l are the same for atomic and molecular vortices, the nature of the vortices (i.e. the spread and the peak density of crests) are different. Molecular vortices are more localized than atomic vortices. The evolution of the population of atoms and molecules with time in two vortex states shows out-of-phase oscillations in both the cases, with and without external decays. However, the amplitude of oscillation decays quickly in the presence of external decay. The out-of-phase oscillation of atomic and molecular numbers in this rotating coupled BEC system shows a signature of coherences as with the coherences present in the evolution of atomic and molecular numbers in the ground state in the absence of any vortices. This coherence is also implemented on the evolution of coupled atomic and molecular ring vortices as their intensity increases or decreases oppositely in the rotating coupled BEC system, both in the presence and absence of external decay. To investigate the feasibility and stability of the atomic and molecular vortices in the rotating coupled BEC system we have studied the lifetime of the system and atom-to-molecular conversion efficiency as a function of laser intensity and the initial number of atoms, considering the external decay. It is found from the lifetime variation that, although the system decays sharply with an increase in laser intensity, the lifetime of the system decreases slowly with an increase in the initial number of atoms. The variation in conversion efficiency shows that it is saturated with an increase in laser intensity, and with an increase in the initial number of atoms it increases steadily. Therefore it can be stated that it is feasible to design coupled atomic and molecular ring vortices in the rotating BEC system depending on the choice of laser intensity and the initial number of atoms. Linear stability analysis reveals that the stability of the coupled atomic and molecular ring vortices can be controlled by changing the system parameters e.g. laser intensity, initial number of atoms, interaction strength and rotation frequency of the system. It is found that the atomic vortices are stable with the variation of these parameters, but the molecular vortices are less stable than the atomic vortices. Therefore the stability of atomic and molecular vortices can be controlled with the optimum choice of the system parameters.

ORCID iDs

Krishna Rai Dastidar https://orcid.org/0000-0002-7132-3021

References

[1] Anderson M H *et al* 1995 *Science* **269** 198
Davis K B, Mewes M O, Andrews M R, van Druten N J, Durfee D S, Kurn D M and Ketterle W 1995 *Phys. Rev. Lett.* **75** 3969
Bradley C C, Sackett C A, Tollet J J and Hulet R G 1995 *Phys. Rev. Lett.* **75** 1687
Han D J, Wynar R H, Courteille P and Heinzen D J 1998 *Phys. Rev.* A **57** R4114
[2] Matthews M R, Anderson B P, Haljan P C, Hall D S, Wieman C E and Cornell E A 1999 *Phys. Rev. Lett.* **83** 2498
Andrews M R, Townsend C G, Miesner H-J, Durfee D S, Kurn D M and Ketterle W 1997 *Science* **275** 637
[3] Dieckmann K, Stan C A, Gupta S, Hadzibabic Z, Schunck C H and Ketterle W 2002 *Phys. Rev. Lett.* **89** 203201
Zwierlein M W, Stan C A, Schunck C H, Raupach S M F, Gupta S, Hadzibabic Z and Ketterle W 2003 *Phys. Rev. Lett.* **91** 250401
[4] Fetter A L and Svidzinsky A A 2001 *J. Phys. Condens. Matter* **13** R135
Mihalache D, Mazilu D, Lederer F, Kartashov Y V, Crasovan L-C, Torner L and Malomed B A 2006 *Phys. Rev. Lett.* **97** 073904
Skarka V, Aleksić N B, Leblond H, Malomed B A and Mihalache D 2010 *Phys. Rev. Lett.* **105** 213901
[5] Theocharis G, Frantzeskakis D J, Kevrekidis P G, Malomed B A and Kivshar Y S 2003 *Phys. Rev. Lett.* **90** 120403
Mertes K M, Merrill J W, Carretero-González R, Frantzeskakis D J, Kevrekidis P G and Hall D S 2007 *Phys. Rev. Lett.* **99** 190402
Scherer M, Lücke B, Gebreyesus G, Topic O, Deuretzbacher F, Ertmer W, Santos L, Arlt J J and Klempt C 2010 *Phys. Rev. Lett.* **105** 135302
Law K J H, Kevrekidis P G and Tuckerman L S 2010 *Phys. Rev. Lett.* **105** 160405
[6] Anderson B P, Haljan P C, Wieman C E and Cornell E A 2000 *Phys. Rev. Lett.* **85** 2857
Madison K W, Chevy F, Wohlleben W and Dalibard J 2000 *Phys. Rev. Lett.* **84** 806
Abo-Shaeer J R, Raman C and Ketterle W 2002 *Phys. Rev. Lett.* **88** 070409
[7] Dalfovo F and Modugno M 2000 *Phys. Rev.* A **61** 023605
Ghosh T K 2004 *Phys. Rev.* A **69** 043606
Carretero-González R, Anderson B P, Kevrekidis P G, Frantzeskakis D J and Weiler C N 2008 *Phys. Rev.* A **77** 033625
Wen L, Xiong H and Wu B 2010 *Phys. Rev.* A **82** 053627
Glatz A, Roberts H L L, Aranson I S and Levin K 2011 *Phys. Rev.* B **84** 180501 (R)
Li J, Wang D-S, Wu Z-Y, Yu Y-M and Liu W-M 2012 *Phys. Rev.* A **86** 023628
Zamora-Zamora R, Lozada-Hidalgo M, Caballero-Benítez S F and Romero-Rochín V 2012 *Phys. Rev.* A **86** 053624
Qin J and Dong G 2016 *Phys. Rev.* A **94** 053611
Haddad L H, O'Hara K M and Carr L D 2015 *Phys. Rev.* A **91** 043609
Li J, Wang D-S, Wu Z-Y, Yu Y-M and Liu W-M 2012 *Phys. Rev.* A **86** 022628
Wang Wenlong, Bisset R N, Ticknor C, Carretero-González R, Frantzeskakis D J, Collins L A and Kevrekidis P G 2017 *Phys. Rev.* A **95** 043638
Seo S W, Ko B, Kim J H, Shin Y and Subramaniyan S 2017 *Phys. Lett.* A **381** 4587
Tsatsos M C, Tavares P E S, Cidrim A, Fritsch A R, Caracanhas M A, Ednilson F, dos Santos A, Barenghi C F and Bagnato V S 2016 *Phys. Rep.* **622**
Madeira L, Caracanhas M A, dos Santos F E A and Bagnato V S 2020 *Annual Review of Condensed Matter Physics* **11** 37–56
[8] Matthews M R, Anderson B P, Haljan P C, Hall D S, Wieman C E and Cornell E A 2000 *Phy. Rev. Lett.* **83** 2498
[9] Kumar R K, Tomio L, Malomed B A and Gammal A 2017 *Phys.Revi.* A **96** 063624
Kato M, Zhang X-F and Saito H 2017 *Phys. Review* A **95** 043605

Toikka L A 2017 *Phys. Rev.* A **96** 033611
Kasamatsu K 2015 *Phy. Rev.* A **92** 063608
Kasamatsu K, Eto M and Nitta M 2016 *Phys. Rev.* A **93** 013615
Tylutki M, Pitaevskii L P, Recati A and Stringari S 2016 *Phys. Rev.* A **93** 043623
Toikka L A and Suominen K-A 2016 *Phys. Rev.* A **93** 053613
Olson A J, Whitenack D L and Chen Y P 2013 *Phys. Rev.* A **88** 043609
Ishino S, Tsubota M and Takeuchi H 2013 *Phys. Rev.* A **88** 063617
Kuopanportti P, Huhtamäki J A M and Möttönen M 2012 *Phys. Rev.* A **85** 043613
Liu C-F, Fan H, Zhang Y-C, Wang D-S and Liu W-M 2012 *Phys. Rev.* A **86** 053616
Eto M, Kasamatsu K, Nitta M, Takeuchi H and Tsubota M 2011 *Phys. Rev.* A **83** 063603
Law K J H, Kevrekidis P G and Tuckerman L S 2010 *Phys. Rev. Letts.* **105** 160405
Kasamatsu K and Tsubota M 2009 *Phys. Rev.* A **79** 023606
Woo S J, Choi S, Baksmaty L O and Bigelow N P 2007 *Phys. Rev.* A **75** 031604R
Catelaniand G and Yuzbashyan E A 2010 *Phys. Rev.* A **81** 033629
Nakamura K, Babajanov D, Matrasulov D and Kobayashi M 2012 *Phys. Rev.* A **86** 053613
Dantas D S, Lima A R P, Chaves A, Almeida C A S, Farias G A and Milošević M V 2015 *Phys. Rev.* A **91** 023630

[10] Thorsheim H R, Weiner J and Julienne P S 1987 *Phys. Rev. Lett.* **58** 2420

[11] Ratliff L P, Wagshul M E, Lett P D, Rolston S L and Phillips W D 1994 *J. Chem. Phys.* **101** 2638
Band Y B and Julienne P S 1995 *Phys. Rev.* A **51** R4317
Jones K M, Tiesinga E, Lett P D and Julienne P S 2006 *Rev. Mod. Phys.* **78** 483
Kuznetsova E, Gacesa M, Pellegrini P, Yelin S F and Côté R 2009 *New J. Phys.* **11** 055028
Koch C P 2008 *Phys. Rev.* A **78** 063411
Koch C P and Shapiro M 2012 *Chem. Rev.* **112** 4928

[12] Wynar R, Freeland R S, Han D J, Ryu C and Heinzen D J 2000 *Science* **287** 1016

[13] Gerton J M, Strekalov D, Prodan I and Hulet R G 2000 *Nature* **408** 692

[14] Donley E A, Claussen N R, Thompson S T and Wieman C E 2002 *Nature* **417** 529

[15] Winkler K, Lang F, Thalhammer G, Straten P V D, Grimm R and Denschlag J H 2007 *Phys. Rev. Lett.* **98** 043201
Mark M *et al* 2005 *Europhys. Lett.* **69** 706

[16] Danzl J G *et al* 2008 *Science* **321** 1062

[17] Jochim S *et al* 2003 *Science* **302** 2101

[18] Drummond P D, Kheruntsyan K V and He H 1998 *Phys. Rev. Lett.* **81** 3055

[19] Heinzen D J, Wynar R, Drummond P D and Kheruntsyan K V 2000 *Phys. Rev. Lett.* **84** 5029

[20] Hope J J and Olsen M K 2001 *Phys. Rev. Lett.* **86** 3220

[21] Gupta M and Dastidar K R 2009 *Phys. Rev.* A **80** 043618
Gupta M and Dastidar K R 2010 *Phys. Rev.* A **81** 033610
Gupta M and Dastidar K R 2008 *J. Phys.* B **41** 195302

[22] de Oliveira F D and Olsen M K 2004 *Opt. Commun.* **234** 235
Yurovsky V A and Ben-Reuven A 2005 *Phys. Rev.* A **72** 053618

[23] Kokkelmans S J J M F, Vissers H M J and Verhaar B J 2001 *Phys. Rev.* A **63** 031601 (R)

[24] Drummond P D, Kheruntsyan K V, Heinzen D J and Wynar R H 2002 *Phys. Rev.* A **65** 063619

[25] Xu X-Q, Lu L-H and Li Y-Q 2009 *Phys. Rev.* A **80** 033621

[26] Ling H Y, Pu H and Seaman B 2004 *Phys. Rev. Lett.* **93** 250403

[27] Cheng J, Han S and Yan Y J 2006 *Phys. Rev.* A **73** 035601

[28] Alexander T J, Kivshar Y S, Ostrovskaya E A and Julienne P S 2002 *J. Opt. B: Quantum Semiclassical Opt.* **4** S33–8
Cusack B J, Alexander T J, Ostrovskaya E A and Kivshar Y S 2001 *Phys. Rev.* A. **65** 013609

[29] Woo S J, Park Q-H and Bigelow N P 2008 *Phys. Rev. Lett.* **100** 120403

[30] Li J, Wang D-S, Wu Z-Y, Yu Y-M and Liu W-M 2012 *Phys. Rev.* A **86** 023628
Yao Y-Q, Li J, Han W, Wang D-S and Liu W-M 2016 *Sci. Rep.* 29566

[31] Bao W and Shen J 2008 *J. Comput. Phys.* **227** 9778